Tokyo Climate Center, Japan Meteorological Agency

TCC News

No. 52 Spring 2018

Contents Page

El Niño Outlook (May – November 2018)

There is a 90% probability that the current La Niña conditions will end in boreal spring and a 70% probability that ENSO-neutral conditions will continue during boreal summer. (Article based on the El Niño outlook issued on 11 May 2018.)

El Niño/La Niña

The NINO.3 SST deviation was -0.5°C in April. The five-month running mean of this deviation was -0.9°C in February 2018, and had remained at -0.5°C or below for six consecutive months before then. SSTs in April were above normal in the western equatorial Pacific and below normal from its central to eastern parts (Figures 1 and 3 (a)). Subsurface temperatures were above normal from western to central parts of the equatorial Pacific and below normal in its eastern part (Figures 2 and 3 (b)). Atmospheric convective activity was below normal near the date line over the equatorial Pacific, and easterly winds in the lower troposphere (trade winds) were above normal over its central part. As these oceanic and atmospheric conditions indicate common features of past La Niña events, La Niña conditions are considered to remain ongoing in the equatorial Pacific.

Eastward migration of subsurface warm waters from western to central parts of the equatorial Pacific was observed in April. These waters are expected to migrate farther eastward to the eastern equatorial Pacific and to weaken lower-than-normal SSTs there. JMA's El Niño prediction model suggests that the NINO.3 SST will be closer to normal during boreal spring (Figure 4). Based on this prediction and the observations detailed above, there is a 90% probability that the five-month running mean NINO.3 SST in May will be between -0.4°C and +0.4°C and a probability of around 70% that this value will persist throughout boreal summer (Figure 5). In conclusion, there is a 90% probability that La Niña conditions will end in boreal spring and a 70% probability that ENSO-neutral conditions will continue during boreal summer.

Western Pacific and Indian Ocean

The area-averaged SST in the tropical western Pacific (NINO.WEST) region was near normal in April. It is likely that values will be below or near normal in boreal summer and autumn.

The area-averaged SST in the tropical Indian Ocean (IOBW) region was below normal in April. It is likely that values will be below or near normal until boreal autumn.

(Shiro Ishizaki, Climate Prediction Division)

* The SST normal for the NINO.3 region (5°S – 5°N, 150°W – 90°W) is defined as an monthly average over the latest sliding 30-year period (1988-2017 for this year).
* The SST normals for the NINO.WEST region (Eq. – 15°N, 130°E – 150°E) and the IOBW region (20°S – 20°N, 40°E – 100°E) are defined as linear extrapolations with respect to the latest sliding 30-year period, in order to remove the effects of significant long-term warming trends observed in these regions.

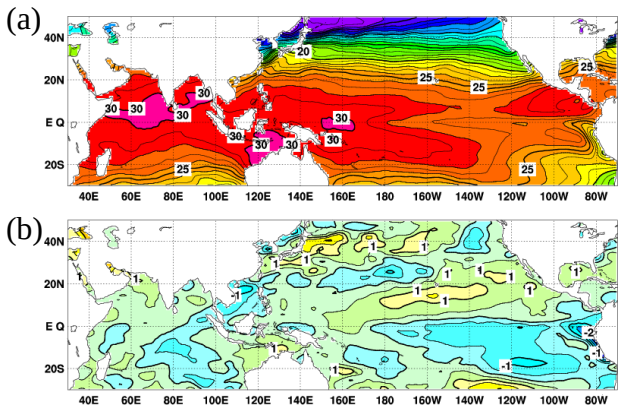

Figure 1 Monthly mean (a) sea surface temperatures (SSTs) and (b) SST anomalies in the Indian and Pacific Ocean areas for April 2018

The contour intervals are 1˚C in (a) and 0.5˚C in (b). The base period for the normal is 1981 – 2010.

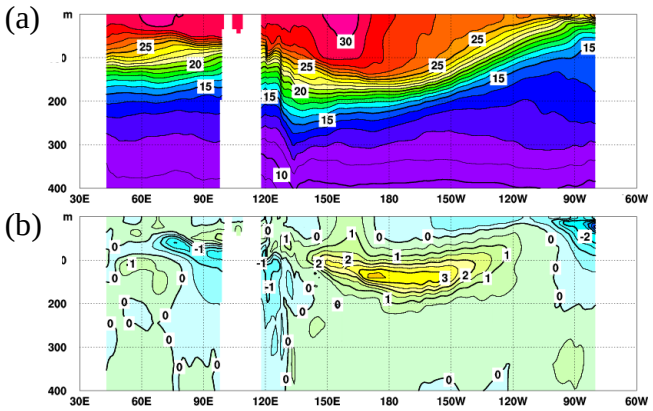

Figure 2 Monthly mean depth-longitude cross sections of (a) temperatures and (b) temperature anomalies in the equatorial Indian and Pacific Ocean areas for April 2018

The contour intervals are 1˚C in (a) and 0.5˚C in (b). The base period for the normal is 1981 – 2010.

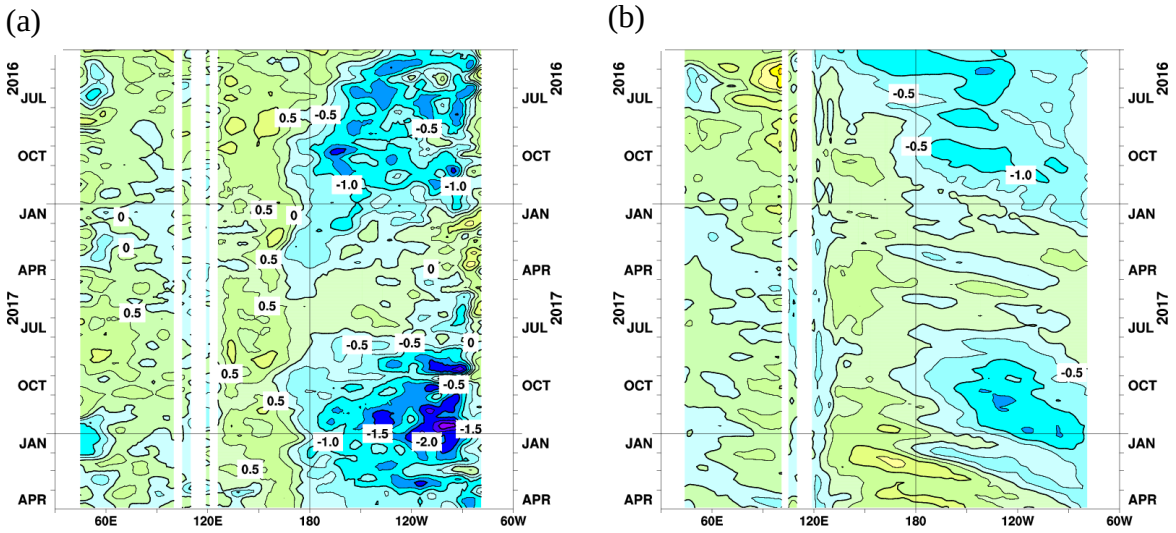

Figure 3 Time-longitude cross sections of (a) SST and (b) ocean heat content (OHC) anomalies along the equator in the Indian and Pacific Ocean areas

OHCs are defined here as vertical averaged temperatures in the top 300 m. The base period for the normal is 1981 – 2010.

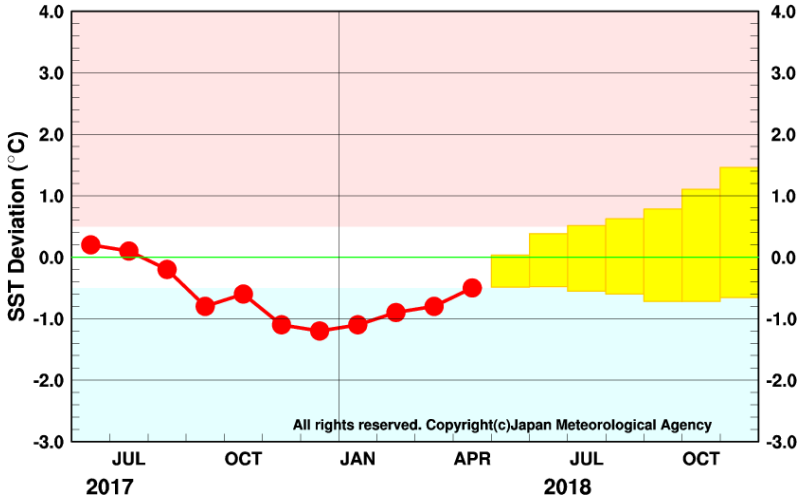

Figure 4 Outlook of NINO.3 SST deviation produced by the El Niño prediction model

This figure shows a time series of monthly NINO.3 SST deviations. The thick line with closed circles shows observed SST deviations, and the boxes show the values produced for up to six months ahead by the El Niño prediction model. Each box denotes the range into which the SST deviation is expected to fall with a probability of 70%.

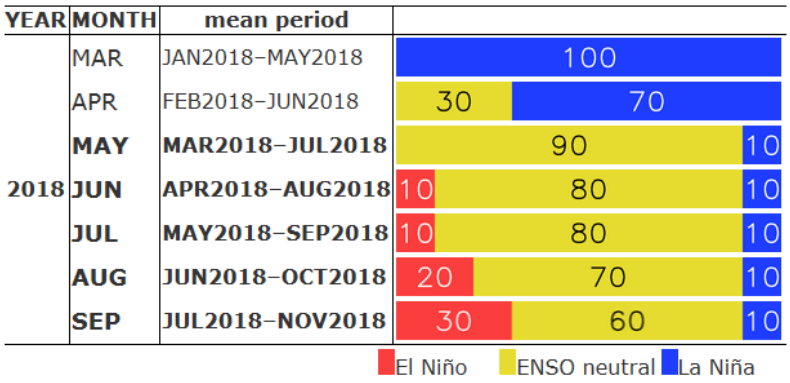

Figure 5 ENSO forecast probabilities based on the El Niño prediction model
Red, yellow and blue bars indicate probabilities that the five-month running mean of the NINO.3 SST deviation from the latest sliding 30-year mean will be +0.5°C or above (El Niño), between +0.4 and -0.4°C (ENSO-neutral) and -0.5°C or below (La Niña), respectively. Regular text indicates past months, and bold text indicates current and future months.

JMA's Seasonal Numerical Ensemble Prediction for Boreal Summer 2018

Based on JMA's seasonal ensemble prediction, sea surface temperature (SST) anomalies in the equatorial Pacific are predicted to remain near normal this boreal summer, suggesting ENSO-neutral conditions. Inactive convection is predicted over the sea east of New Guinea in association with below-normal SST conditions, while active convection is predicted over the sea south of Hawaii in association with remarkably higher-than-normal SST conditions. Focusing on Asia, precipitation is predicted to be above normal over most of South Asia, suggesting an active Asian Monsoon.

1. Introduction

This article outlines JMA's dynamical seasonal ensemble prediction for boreal summer 2018 (June – August, referred to as JJA), which was used as a basis for JMA's operational warm-season outlook issued on 25 May 2018. The outlook is based on the seasonal ensemble prediction system of the Coupled Atmosphere-ocean General Circulation Model (CGCM). See the column below for system details.

Section 2 outlines global SST anomaly predictions, and Section 3 describes the associated circulation field predictions for the tropics and sub-tropics. Finally, the circulation fields predicted for the mid- and high latitudes of the Northern Hemisphere are discussed in Section 4.

2. SST anomalies (Figure 6)

Figure 6 shows predicted SSTs (contours) and related anomalies (shading) for JJA. SST anomalies in the equatorial Pacific are predicted to remain near normal this boreal summer, suggesting ENSO-neutral conditions. Meanwhile, SST conditions are predicted to be remarkably higher than normal in the sea south of Hawaii and near normal in the Indian Ocean.

3. Prediction for the tropics and sub-tropics (Figure 7)

Figure 7 (a) shows predicted precipitation (contours) and related anomalies (shading) for JJA. Below-normal anomalies are predicted over the sea east of New Guinea in association with below-normal SST conditions in the wake of the terminated La Niña event. Above-normal anomalies are predicted over the sea south of Hawaii in association with remarkably higher-than-normal SST conditions. Focusing on Asia, above-normal anomalies are predicted over most parts of South Asia, reflecting an active Asian Monsoon.

Figure 7 (b) shows predicted velocity potential (contours) and related anomalies (shading) at the upper troposphere (200 hPa) for JJA. Positive (i.e., convergent) anomalies are predicted over the sea east of New Guinea in association with light precipitation, while negative (i.e., divergent) anomalies are predicted over the sea south of Hawaii in association with heavy precipitation.

Figure 7 (c) shows predicted stream functions (contours) and related anomalies (shading) at the upper troposphere (200 hPa) for JJA. Positive (i.e., anticyclonic) anomalies are predicted over the sea around Hawaii in association with active convection over the sea south of Hawaii. Positive (i.e., anticyclonic) anomalies are also predicted over Central Asia and the northern parts of Japan in association with an active Asian Monsoon and an active convection over the sea southeast of Japan respectively, suggesting an enhanced Tibetan High.

Figure 7 (d) shows predicted stream functions (contours) and related anomalies (shading) at the lower troposphere (850 hPa) for JJA. Negative (i.e., cyclonic) anomalies are predicted over the sea southeast of Japan, suggesting a weaker-than-normal North Pacific High.

4. Prediction for the mid- and high- latitudes of the Northern Hemisphere

Figure 8 (a) shows predicted geopotential heights (contours) and related anomalies (shading) at 500 hPa for JJA. Positive anomalies are predicted over most of the Northern Hemisphere, reflecting high thickness caused by active convection over the North Pacific and global warming trends.

Figure 8 (b) shows predicted sea level pressure (contours) and related anomalies (shading) for JJA. Positive anomalies are predicted over the northern parts of Japan, suggesting a stronger-than-normal North Pacific High. Negative anomalies are predicted over the sea southeast of Japan, suggesting a weaker-than-normal North Pacific High.

.

(Takashi Yamada, Climate Prediction Division)

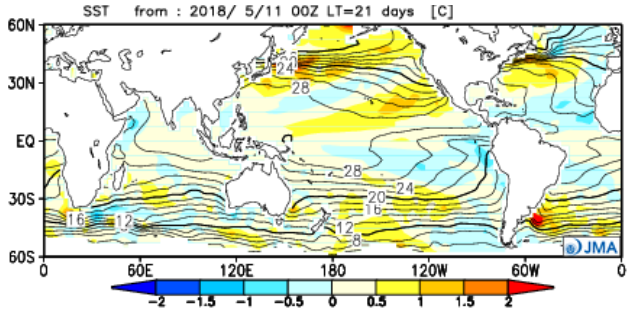

Figure 6 Predicted SSTs (contours) and SST anomalies (shading) for June–August 2018 (ensemble mean of 51 members)

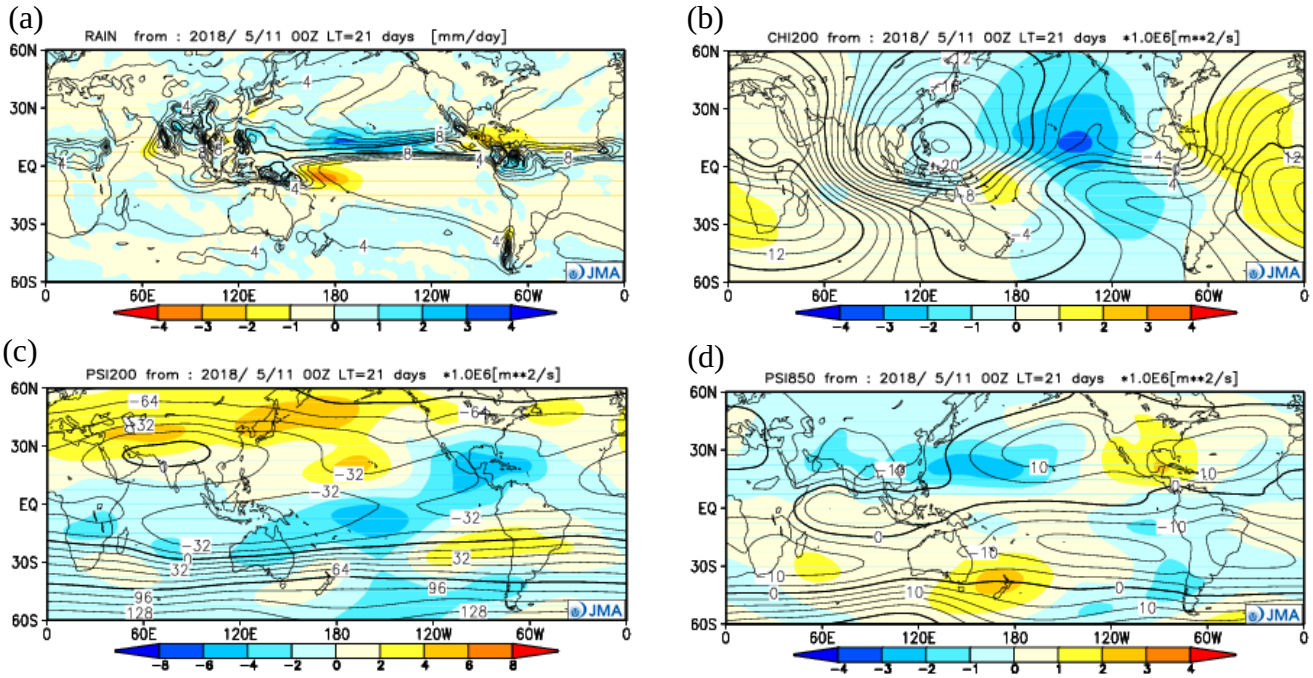

Figure 7 Predicted atmospheric fields from 60°N – 60°S for June–August 2018 (ensemble mean of 51 members)
(a) Precipitation (contours) and anomaly (shading). The contour interval is 2 mm/day.
(b) Velocity potential at 200 hPa (contours) and anomaly (shading). The contour interval is 2×10^6 m^2/s.
(c) Stream function at 200 hPa (contours) and anomaly (shading). The contour interval is 16×10^6 m^2/s.
(d) Stream function at 850 hPa (contours) and anomaly (shading). The contour interval is 5×10^6 m^2/s.

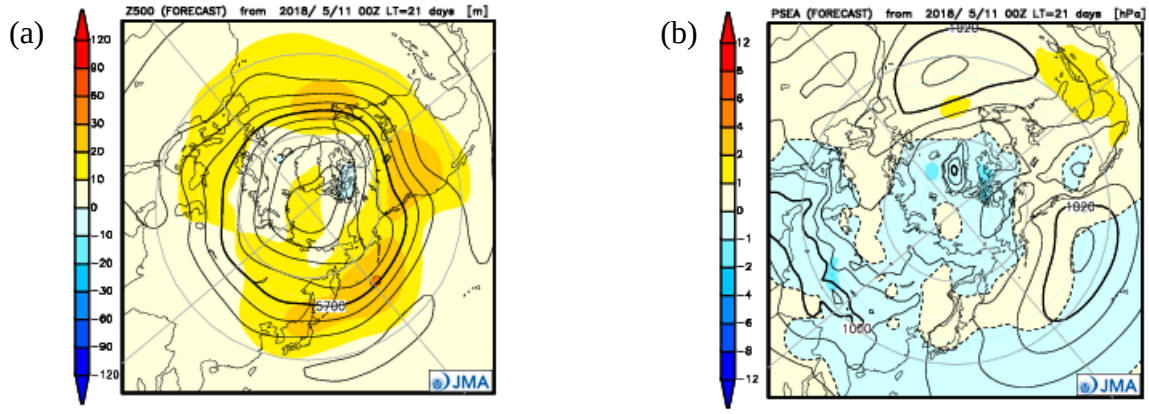

Figures 8 Predicted atmospheric fields from 20°N – 90°N for June–August 2018 (ensemble mean of 51 members)
(a) Geopotential height at 500 hPa (contours) and anomaly (shading). The contour interval is 60 m.
(b) Sea level pressure (contours) and anomaly (shading). The contour interval is 4 hPa.

JMA's Seasonal Ensemble Prediction System

JMA operates a seasonal Ensemble Prediction System (EPS) using the Coupled atmosphere-ocean General Circulation Model (CGCM) to make seasonal predictions beyond a one-month time range. The EPS produces perturbed initial conditions by means of a combination of the initial perturbation method and the lagged average forecasting (LAF) method. The prediction is made using 51 members from the latest four initial dates (13 members are run every 5 days). Details of the prediction system and verification maps based on 30-year hindcast experiments (1981–2010) are available at http://ds.data.jma.go.jp/tcc/tcc/products/model/.

Warm Season Outlook for Summer 2018 in Japan

JMA issued warm season outlook for the coming summer (June – August) over Japan in February and updated it on 25 May 2018. This article outlines the update.

1. Outlook summary (Figure 9)

- Seasonal mean temperatures are expected to be above-normal all over Japan.
- Seasonal precipitation amounts are expected to exhibit a below-normal tendency in Okinawa.

2. Outlook background

Figure 10 summarizes expected large-scale oceanic/atmospheric characteristics for the coming summer. The grounds for the outlook are given below.

- The current La Niña conditions are likely to end in spring, and neutral conditions are likely during summer. SSTs over many parts from North Indian Ocean to the North Pacific are expected to be above normal.
- Convective activity is expected to be enhanced over most of the Asian Monsoon region due in part to higher SSTs.
- In the upper troposphere, the subtropical jet stream over Asia is expected to shift northward. The Tibetan High is expected to be strong in its northern part and extend toward Japan due to the enhanced Asian Monsoon.
- In the sea level pressure field, negative anomalies are expected to the east of the Philippines due to enhanced convective activity in the region. Positive anomalies are expected over Japan, suggesting an expansion of the North Pacific High toward the country.
- The extension of the North Pacific High over Japan may bring drier conditions in Okinawa/Amami, while moist air could flow over northern Japan along the periphery of the high.
- Overall temperatures in the troposphere are expected to be above normal due to the prevailing long-term increasing trend. These tendencies are likely to increase the chance of above-normal temperatures.

(Hiroshi Ohno, Climate Prediction Division)

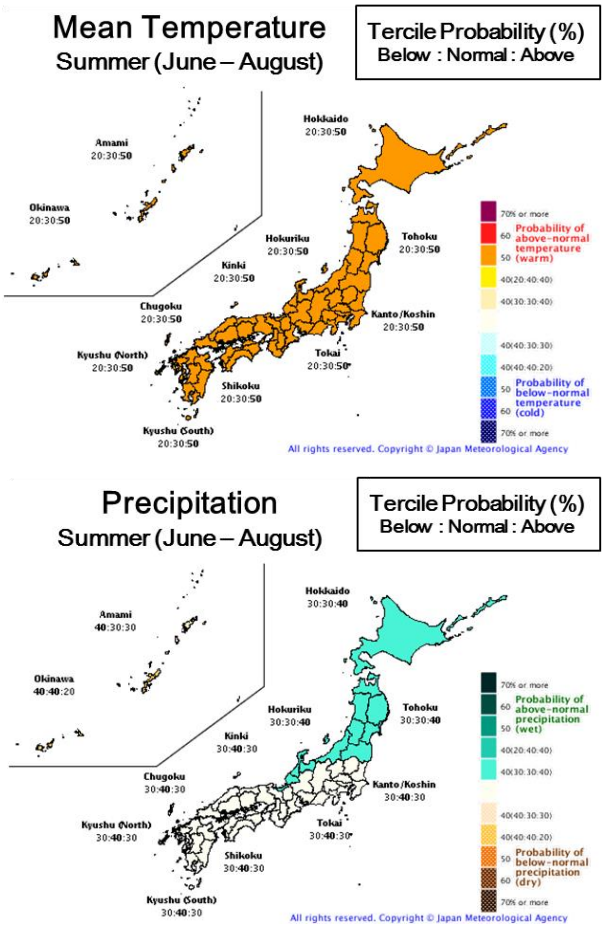

Figure 9: Outlook for summer 2018 temperature (top) and precipitation (bottom) probability in Japan

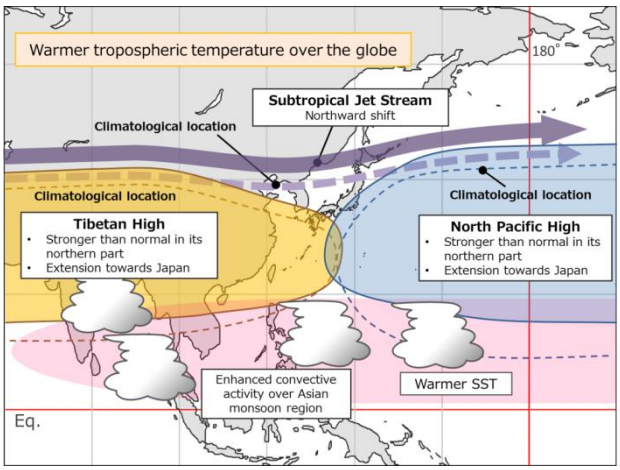

Figure 10: Conceptual diagram showing expected large-scale ocean/atmosphere characteristics for summer 2018

Summary of the 2017/2018 Asian Winter Monsoon

This report summarizes the characteristics of the surface climate and atmospheric/oceanographic considerations related to the Asian winter monsoon for 2017/2018.

Note: The Japanese 55-year Reanalysis (JRA-55; Kobayashi et al. 2015) atmospheric circulation data and COBE-SST (Ishii et al. 2005) sea surface temperature (SST) data were used for this investigation. The outgoing longwave radiation (OLR) data referenced to infer tropical convective activity were originally provided by NOAA. The base period for the normal is 1981 – 2010. The term "anomaly" as used in this report refers to deviation from the normal.

1. Surface climate conditions

Temperature anomalies in Asia for boreal winter 2017/2018 were generally high both north of 60°N and south of 30°N, and were low in the latitudinal band between 30 and 60°N (Figure 11). In particular, the eastern part of East Asia experienced lower-than-normal temperatures as often observed in La Niña winters. Three-month mean temperatures for December 2017 to February 2018 were extremely high from eastern to central parts of Eastern Siberia and in the northern part of Western Siberia. Precipitation amounts during this period were above normal in Southeast Asia and from the western part of Eastern Siberia to Central Siberia, and were below normal from eastern to southern parts of East Asia and in and around India (Figure 12). The wetter-than-normal conditions observed in Southeast Asia were consistent with typical anomaly patterns observed in past La Niña events. Three-month mean precipitation amounts for December 2017 to February 2018 were extremely high in and around southern Central Siberia.

Figure 13 shows extreme climate conditions observed between December 2017 and February 2018. In December, extremely high temperatures were seen in the northeastern part of Eastern Siberia and in and around southwestern China. Extremely high precipitation amounts were observed from the southern part of Central Siberia to northwestern Mongolia.

In January, extremely high temperatures were seen in the eastern part of Eastern Siberia, and extremely low temperatures were seen from central Mongolia to eastern Kazakhstan. Extremely high precipitation amounts were observed in and around the central part of the Philippines, the southern Malay Peninsula and central Mongolia, while extremely low precipitation amounts were observed in and around the southeastern part of Central Asia. In February, extremely high temperatures were seen in Eastern Siberia and in and around the northeastern part of Southeast Asia.

2. Characteristic atmospheric circulation and oceanographic conditions

2.1 Conditions in the tropics

The La Niña conditions that emerged in boreal autumn 2017 matured in winter 2017/2018. Remarkably positive SST anomalies were observed in the western equatorial Pacific and negative SST anomalies were observed from central to eastern parts of the equatorial Pacific (Figure 14), as often seen during La Niña events.

An active convection phase of the Madden-Julian Oscillation (MJO) propagated eastward from the Indian Ocean to the Maritime Continent in January (Figure 15). Convective activity inferred from OLR during this period was enhanced from the Indochina Peninsula to the seas east of the Philippines and was suppressed over the equatorial Indian Ocean and from the west of the date line to the central equatorial Pacific (Figure 16 (a)), which is also typical of La Niña episodes. Over the Maritime Continent, convective activity was enhanced in January (Figure 16 (c)), and weakened in February in association with eastward propagation of the MJO phase (Figure 16 (d)).

In the upper troposphere, clear large-scale divergent anomalies were seen over the western Pacific in association with enhanced convective activity, and convergent anomalies were observed over the Middle East (Figure 17 (a)). In the 200-hPa stream function field, a wave train stretched from Northern Africa to the northern part of East Asia with anti-cyclonic circulation anomalies extending from eastern India to southern China (Figure 17 (b)).

In the lower troposphere, cyclonic circulation anomalies straddling the equator were seen from the Indian Ocean to the Maritime Continent (Figure 17 (c)).

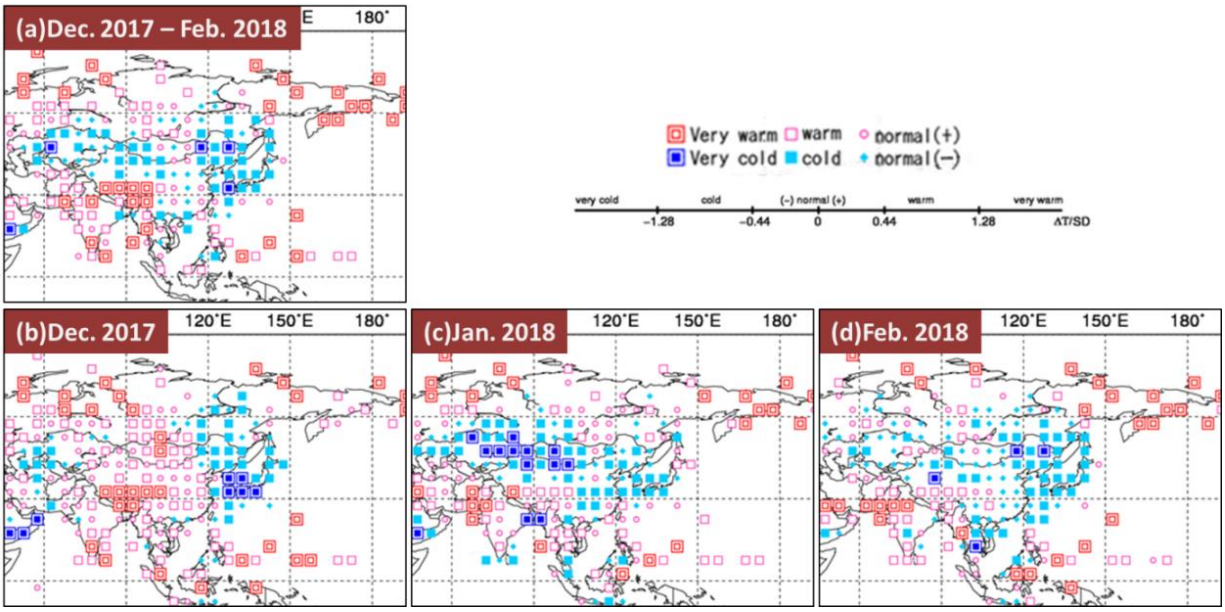

Figure 11 (a) Three-month mean temperature anomalies for December 2017 to February 2018, and monthly mean temperature anomalies for (b) December 2017, (c) January 2018 and (d) February 2018
Categories are defined by the three-month/monthly mean temperature anomaly against the normal divided by its standard deviation and averaged in 5° × 5° grid boxes. The thresholds of each category are -1.28, -0.44, 0, +0.44 and +1.28. Standard deviations were calculated from 1981 - 2010 statistics. Areas over land without graphical marks are those where observation data are insufficient or where normal data are unavailable.

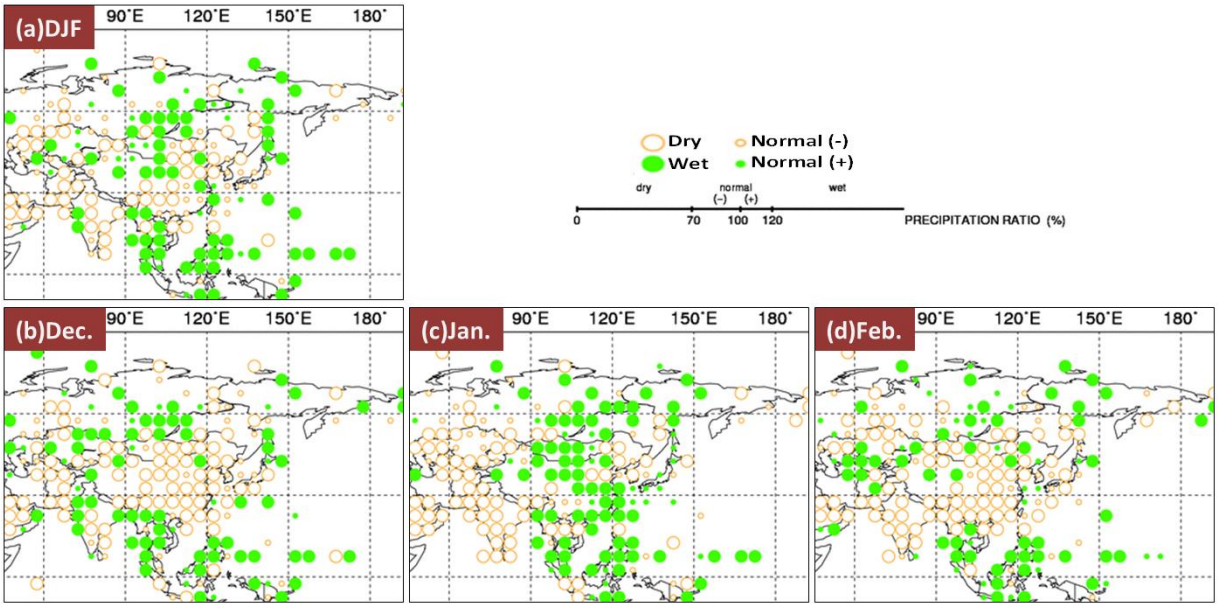

Figure 12 Three-month total precipitation ratio for December 2017 to February 2018, and monthly total precipitation ratio for (b) December 2017, (c) January 2018 and (d) February 2018
Categories are defined by the three-month mean precipitation ratio against the normal and averaged in 5° × 5° grid boxes. The thresholds of each category are 70, 100 and 120%. Areas over land without graphical marks are those where observation data are insufficient or where normal data are unavailable.

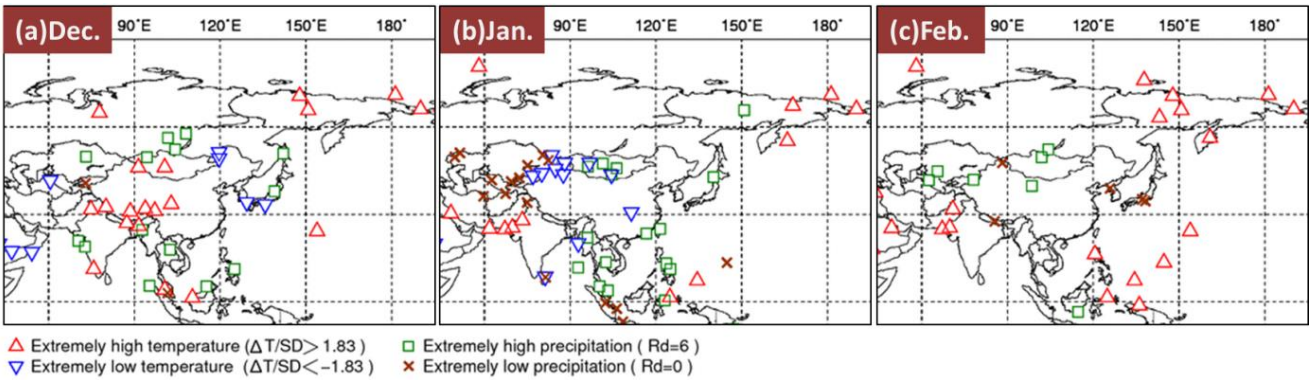

Figure 13 Extreme climate stations for (a) December 2017, (b) January 2018 and (c) February 2018
ΔT, SD and Rd indicate temperature anomaly, standard deviation and quintile, respectively.

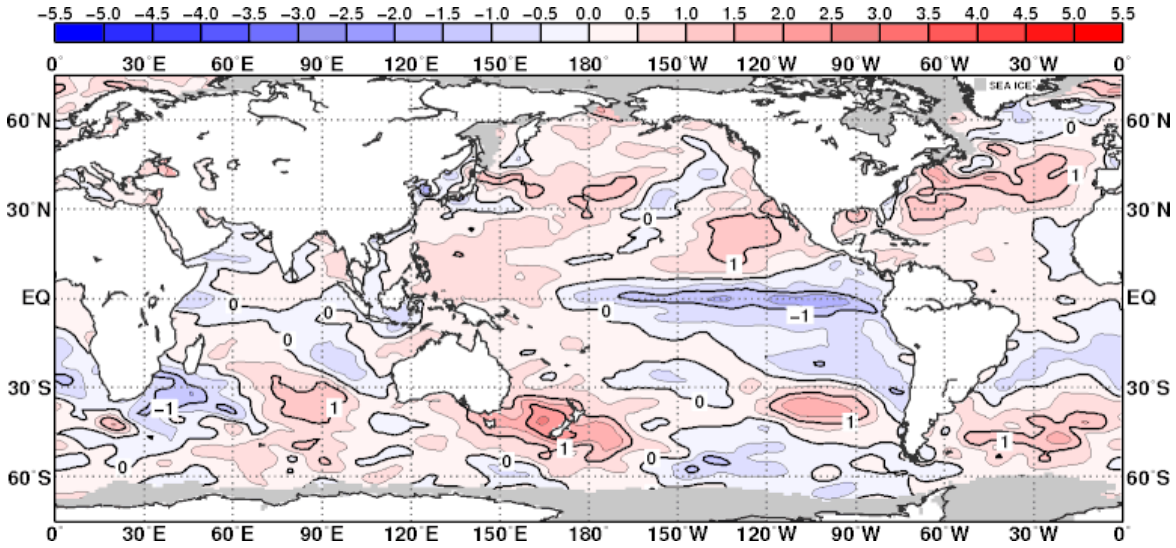

Figure 14 Three-month mean sea surface temperature (SST) anomalies for December 2017 to February 2018
The contour interval is 0.5˚C.

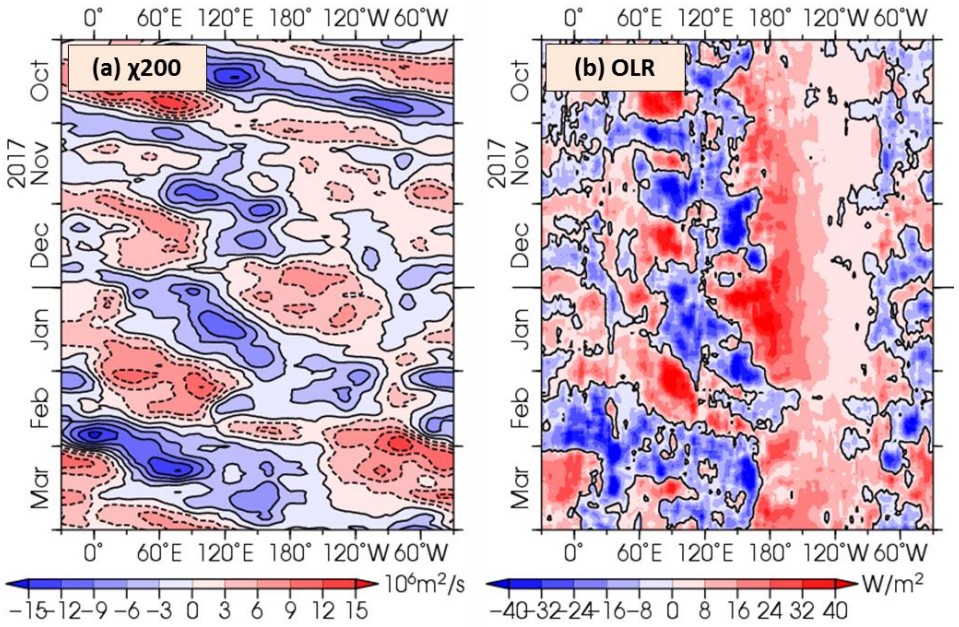

Figure 15 Time-longitude cross section of seven-day running mean (a) 200-hPa velocity potential anomalies, and (b) outgoing longwave radiation (OLR) anomalies around the equator (5°S – 5°N) for October 2017 to March 2018
(a) The blue and red shading indicates areas of divergence and convergence anomalies, respectively. (b) The blue and red shading indicates areas of enhanced and suppressed convective activity, respectively.

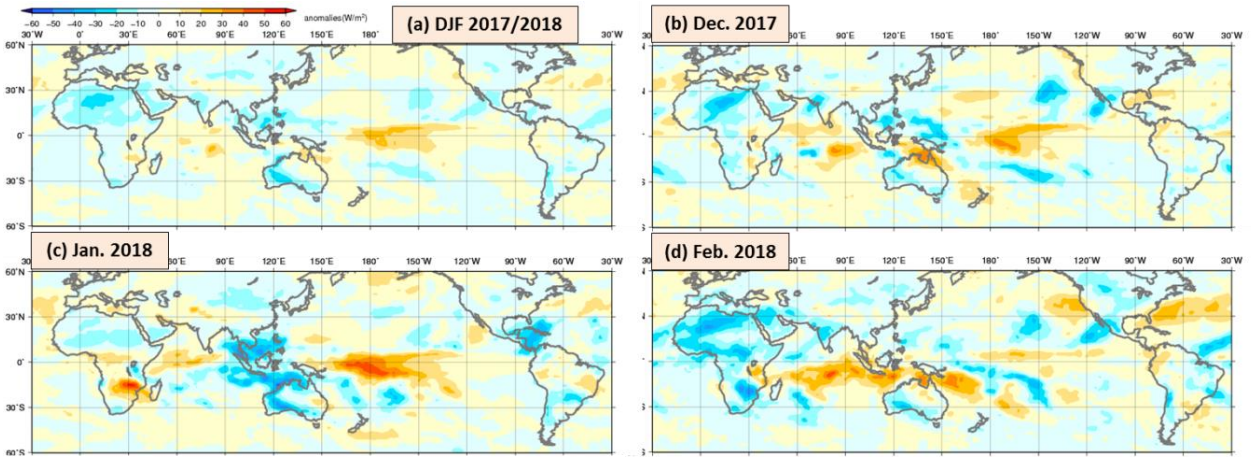

Figure 16 Outgoing longwave radiation (OLR) anomalies (a) averaged over the three months from December 2017 to February 2018, for (b) December 2017, (c) January 2018 and (d) February 2018
The blue and red shading indicates areas of enhanced and suppressed convective activity, respectively.

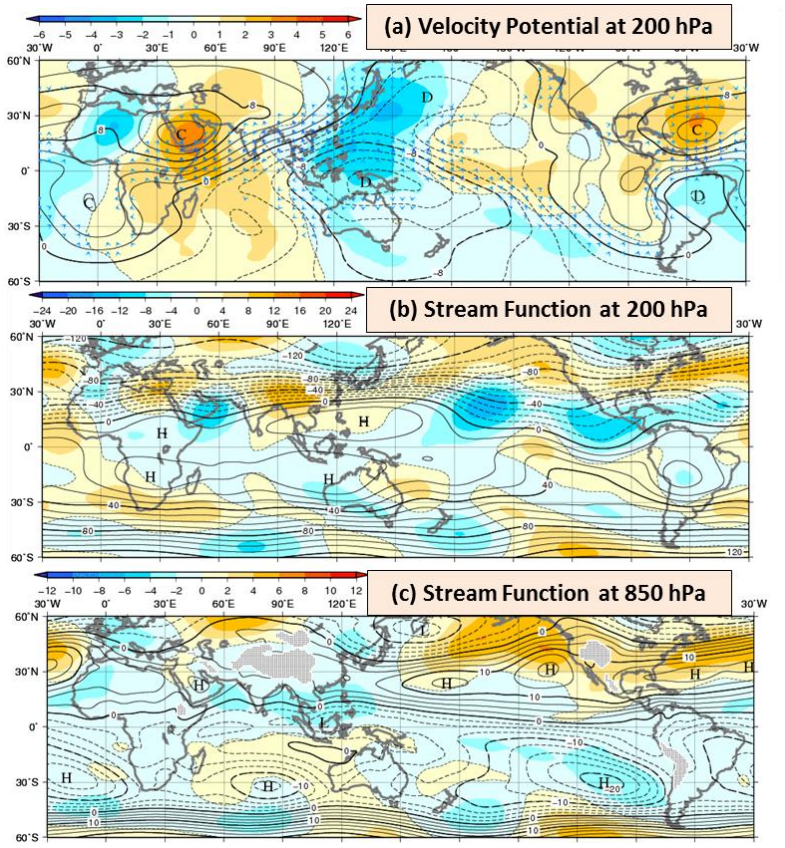

Figure 17 Three-month mean (a) 200-hPa velocity potential, (b) 200-hPa stream function, and (c) 850-hPa stream function for December 2017 to February 2018 (unit: 10^6 m^2/s)
(a) The contours indicate velocity potential at intervals of 2×10^6 m^2/s, and the shading shows velocity potential anomalies. D and C indicate the bottom and the peak of velocity potential, corresponding to the centers of large-scale divergence and convergence, respectively. (b, c) The contours indicate stream function at intervals of (b) 10 and (c) 2.5×10^6 m^2/s, and the shading shows stream function anomalies. H and L denote the centers of anticyclonic and cyclonic circulations, respectively.

2.2 Conditions in the extratropics

In the 500-hPa height field during winter 2017/2018 (Figure 18 (a)), the polar vortex in the Northern Hemisphere split into an Eastern Siberian part and a North American part in association with positive height anomalies over and around the North Pole. A clear wave train was observed over northern Eurasia, corresponding to the positive Eurasian (EU) teleconnection pattern (Wallace and Gutzler, 1982). The subtropical jet stream over Eurasia was displaced northward of its normal position in general while meandering northward over China and southward over Japan (Figure 19 (a)).

In the sea level pressure field (Figure 20 (a)), the Siberian High was stronger than normal in general. The Aleutian Low was shifted westward and was stronger than normal over and around the Kamchatka Peninsula. Temperatures at 850-hPa (Figure 21 (a)) were below normal over East Asia.

2.3 Primary factors contributing to the characteristics of the 2017/2018 Asian Winter Monsoon

Convective activity was enhanced over the Maritime Continent due to higher-than-normal SSTs in the tropical western Pacific region in association with the La Niña event observed from boreal autumn 2017 onward (Figure 14 and Figure 15 (a)). This enhanced convection strengthened the northwestward expansion of an upper-level high over the area from the South China Sea to the east of the Philippines (Figure 16 (a)), which in turn excited a Rossby wave, causing southward meandering of the subtropical jet stream around Japan (Figure 19 (a)).

The tropospheric polar vortex split in association with significant meandering of the polar-front jet stream over northern Eurasia caused by a blocking high over Western Siberia and other influences. One of the polar vortex sections shifted southward over Eastern Siberia (Figure 18 (a)), which caused southward meandering of the polar-front jet stream over the eastern part of East Asia.

Meandering of the subtropical and polar-front jet streams was also caused by Rossby wave packet propagation that can be traced back to the upper-level ridge over the North Atlantic (Figure 22).

As a result, northerly cold air flowed over the eastern part of East Asia more frequently than in normal winters, contributing to low temperatures in the region (Figure 11, Figure 21). There was a tendency for cold-air masses to flow over Japan, bringing intermittent heavy snowfall to some parts of the country.

(Hiroki Togawa, Climate Prediction Division)

References

Ishii, M., A. Shouji, S. Sugimoto and T. Matsumoto, 2005: Objective Analyses of Sea-Surface Temperature and Marine Meteorological Variables for the 20th Century using ICOADS and the Kobe Collection. Int. *J. Climatol.*, **25**, 865-879.

Kobayashi, S., Y. Ota, Y. Harada, A. Ebita, M. Moriya, H. Onoda, K. Onogi, H. Kamahori, C. Kobayashi, H. Endo, K. Miyaoka, and K. Takahashi, 2015: The JRA-55 Reanalysis: General Specifications and Basic Characteristics. *J. Meteorol. Soc.* Japan, **93**, 5 – 48.

Takaya, K., and H. Nakamura, 2001: A Formulation of a Phase-Independent Wave-Activity Flux for Stationary and Migratory Quasigeostrophic Eddies on a Zonally Varying Basic Flow. *J. Atmos. Sci.*, **58**, 608-627.

Wallace, J.M., and D.S. Gutzler, 1981: Teleconnections inthe Geopotential Height Field during the Northern Hemisphere Winter. *Mon. wea. Rev.*, **109**, 784-812.

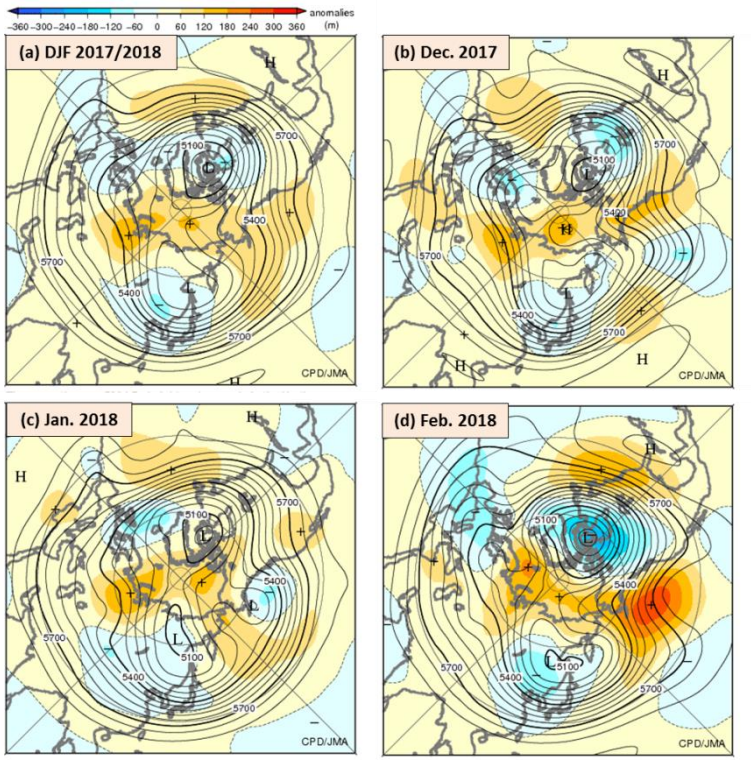

Figure 18 500-hPa height (a) averaged over the three months from December 2017 to February 2018, for (b) December 2017, (c) January 2018, and (d) February 2018
The contours indicate 500-hPa height at intervals of 60 m, and the shading denotes anomalies. H and L indicate the peak and bottom of 500-hPa height, respectively, and + (plus) and – (minus) show the peak and bottom of anomalies, respectively.

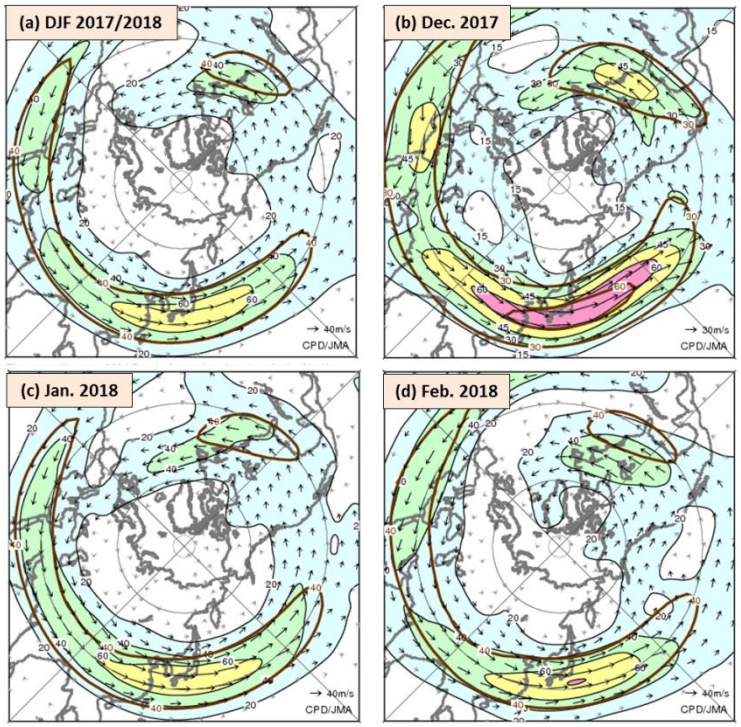

Figure 19 200-hPa wind speed and vectors (a) averaged over the three months from December 2017 to February 2018, for (b) December 2017, and (c) January 2018 and (d) February 2018

The black lines show wind speed at intervals of 20 m/s for (a), (c) and (d), and 15 m/s for (b). The brown lines show its normal at intervals of 40 m/s for (a), (c) and (d), and 30 m/s for (b). The base period for the normal is 1981 - 2010.

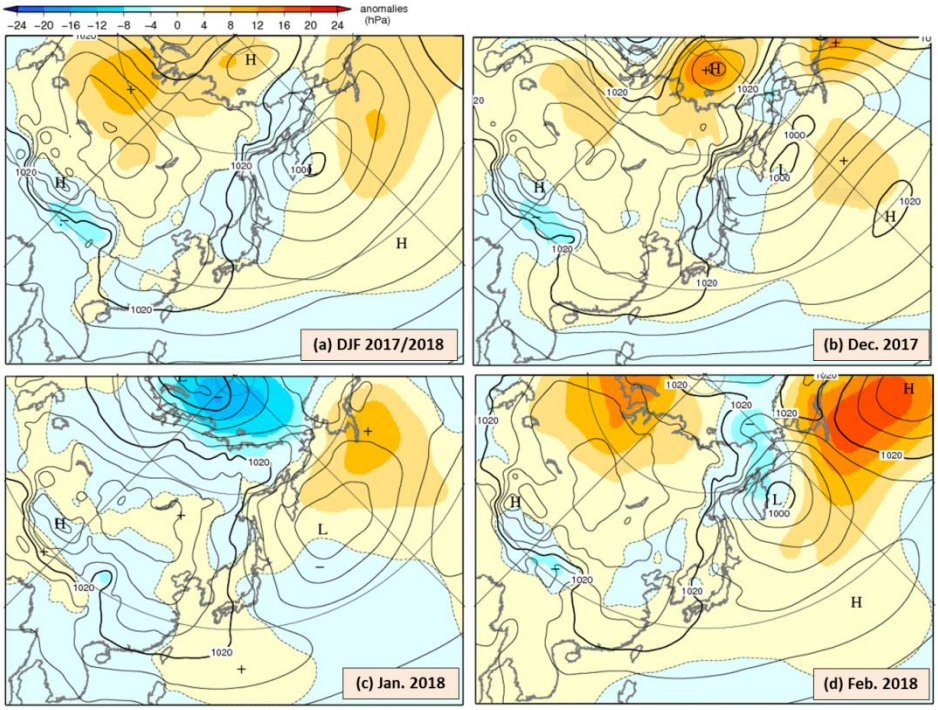

Figure 20 Sea level pressure (a) averaged over the three months from December 2017 to February 2018, for (b) December 2017, (c) January 2018 and (d) February 2018

The contours indicate sea level pressure at intervals of 4 hPa, and the shading shows related anomalies. H and L indicate the centers of high and low pressure systems, respectively, and + (plus) and – (minus) show the peak and bottom of sea level pressure anomalies, respectively.

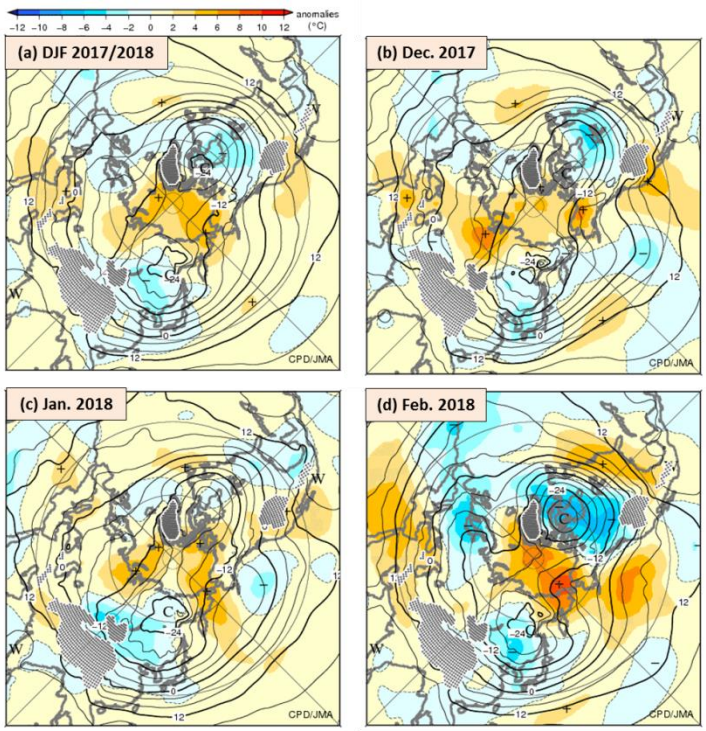

Figure 21 850-hPa temperature (a) averaged over the three months from December 2017 to February 2018, for (b) December 2017, (c) January 2018 and (d) February 2018

The contours indicate 850-hPa temperature at intervals of 4 °C and the shading shows related anomalies.

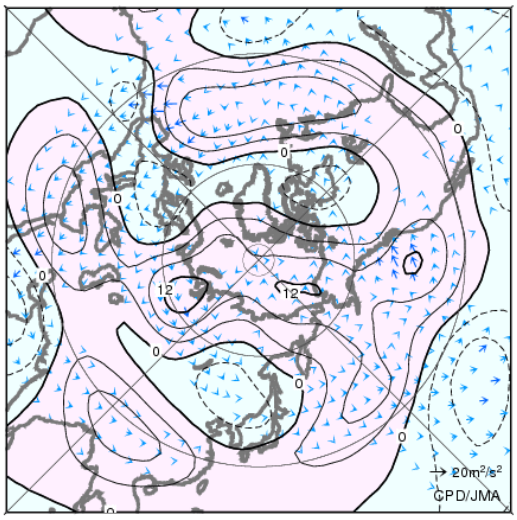

Figure 22 300-hPa stream function anomaly and wave activity flux averaged over the three months from December 2017 to February 2018

The counters indicate stream function anomalies at intervals of 4×10^6 m^2/s, and the vectors show wave activity flux (unit: m^2/s^2). The vectors are not shown where wave activity flux is less than 2 m^2/s^2. The wave activity flux was calculated with reference to Takaya and Nakamura (2001).

Characteristics of climate conditions in Japan in winter 2017/18

1. Climate conditions

A series of extreme cold spells hit Japan and its surrounding areas in winter 2017/18, and cold air consequently prevailed nationwide (Figure 23). The seasonal mean temperature anomaly in western Japan was -1.2°C (Figure 24), which was the lowest for 32 years since the 1985/86 value of -2.1°C.

Some parts of the country intermittently experienced heavy snowfall associated with cold-spell peaks, leading to unprecedented snow depths at some weather stations (Figure 25). Annual snow depth records were equaled or broken at 17 of 321 JMA stations where snow gauges are operated.

2. Primary factors

The primary factors contributing the climate conditions detailed above are illustrated in Figure 26. Figure 27 is as per Figure 26, but for a severe cold-wave event occurring in early February 2018.

- The series of extreme cold spells hitting Japan during this winter period were attributable to a tendency for the subtropical and polar front jet streams to meander southward around the country along with a strengthened northwesterly monsoon.
- The southward meandering of the subtropical jet stream was partly attributable to enhanced convective activity over the Maritime Continent in association with the La Niña event observed from boreal autumn 2017 onward (see the press release Cold Waves and Heavy Snow in Japan from December 2017 dated 23rd February 2018). This meandering was also probably attributable to Rossby wave packet propagation that can be traced back to a persistent upper-level ridge over the North Atlantic.
- The southward meandering of the polar front jet stream occurred partly because the tropospheric polar vortex split and one of the pieces shifted southward over eastern Siberia. This splitting was associated with large meandering of the polar front jet stream over northern Eurasia.
- This meandering over northern Eurasia was attributable to the persistent upper-level ridge over the North Atlantic and possibly to lower-than-normal sea ice extents in the Barents Sea and the Kara Sea as seen in previous studies (e.g., Mori et al. 2014).

See also "Seasonal Highlights on the Climate System (December 2017 – February 2018)" on the TCC website.

[Note]

This summary report is based on analysis and discussion in an ordinary session of the TCC Advisory Panel on Extreme Climatic Events on 5 March 2018. The Panel, consisting of prominent experts on climate science from universities and research institutes, was established in June 2007 by JMA to investigate extreme climate events based on up-to-date information and findings. The current chair is Prof. Hisashi Nakamura from the University of Tokyo. See TCC News No. 28 for more details on the outline and the framework of the Panel.

References

Mori, M., M. Watanabe, H. Shiogama, J. Inoue, and M. Kimoto, 2014: Robust Arctic sea-ice influence on the frequent Eurasian cold winters in past decades. *Nat. Geosci.* **7**, 869–873.

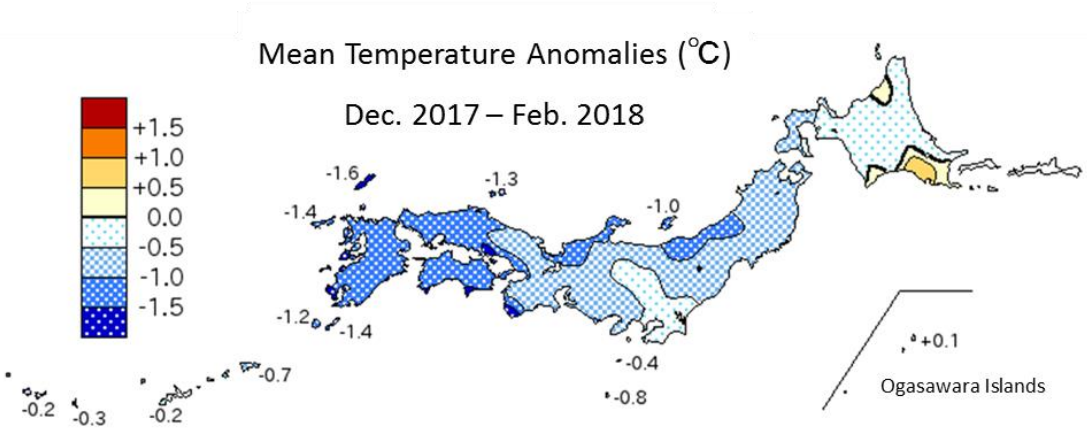

Figure 23. Seasonal mean temperature anomalies for winter 2017/18 (December 2017 – February 2018)
The base period for the normal is 1981– 2010.

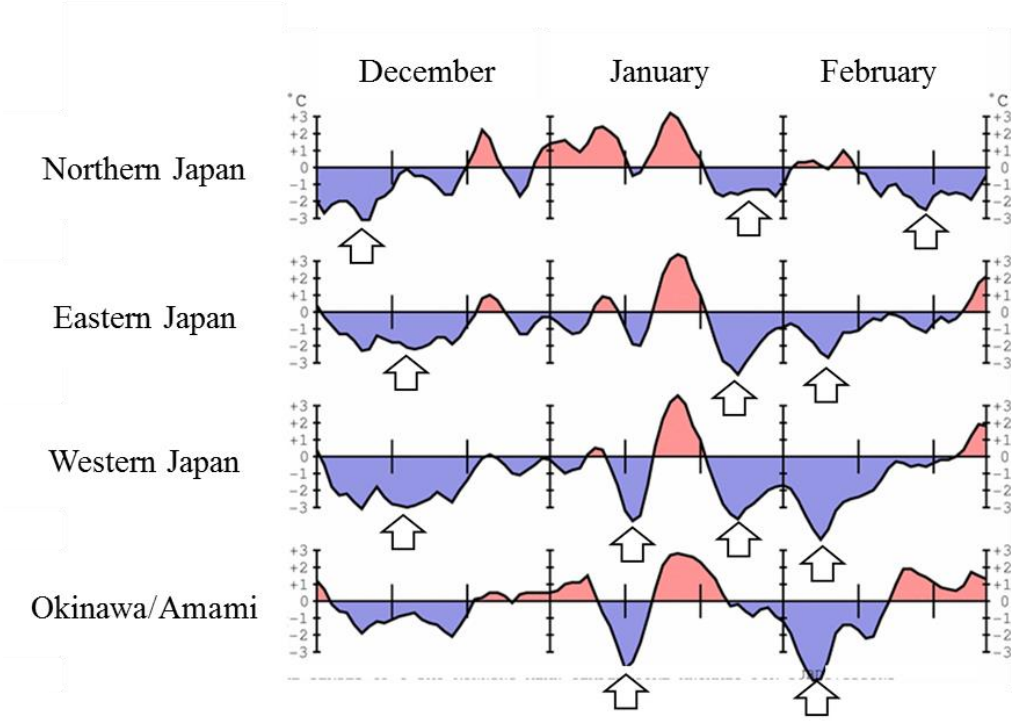

Figure 24. Time-series representations of 5-day running mean temperature anomalies [°C] from December 2017 to February 2018

The base period for the normal is 1981– 2010. Arrows indicate peak low temperatures. For more details of the cold spell in late January, see the press release Cold Spell in Japan from late January 2018 dated February 2, 2018.

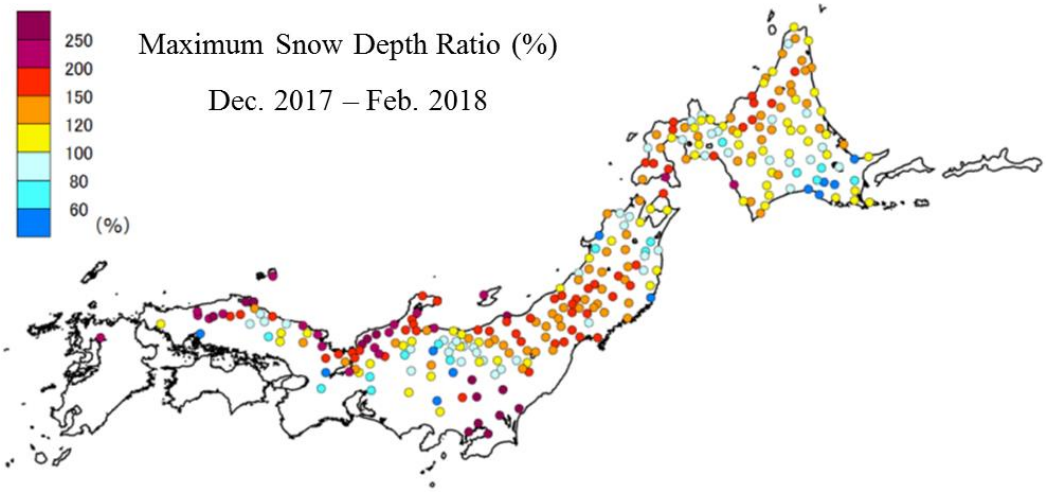

Figure 25 Maximum snow depth ratios to the normal during winter 2017/18

The base period for the normal is 1981– 2010.

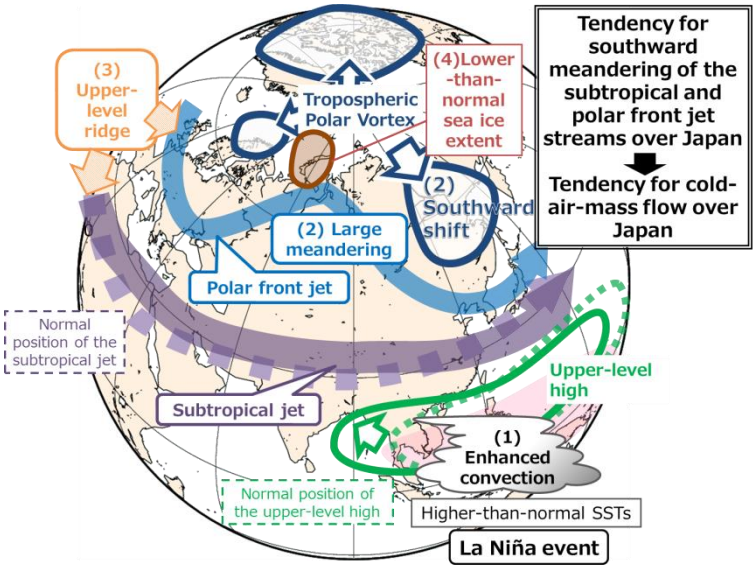

Figure 26 Primary factors contributing to climate conditions in Japan in winter 2017/18

The numbered events in Figure 26 are described in further detail below.

(1) Convective activity was enhanced over the Maritime Continent due to higher-than-normal SSTs in the tropical western Pacific region in association with the La Niña event observed from boreal autumn 2017 onward. This enhanced convection strengthened northwestward expansion of an upper-level high located over the area from the South China Sea to the east of the Philippines, which excited a Rossby wave causing the southward meandering of the subtropical jet stream around Japan.

(2) The tropospheric polar vortex split in association with large meandering of the polar front jet stream over northern Eurasia, which was caused by a blocking high over western Siberia and other influences. One of the polar vortex pieces shifted southward over eastern Siberia, which caused the southward meandering of the polar front jet stream around Japan.

(3) The meandering of the subtropical and the polar front jet streams as mentioned in (1) and (2), respectively, was also caused by Rossby wave packet propagation that can be traced back to the upper-level ridge over the North Atlantic.

(4) Sea ice extents in the Barents Sea and the Kara Sea were lower than normal, which may have caused the meandering of the polar front jet stream over Eurasia.

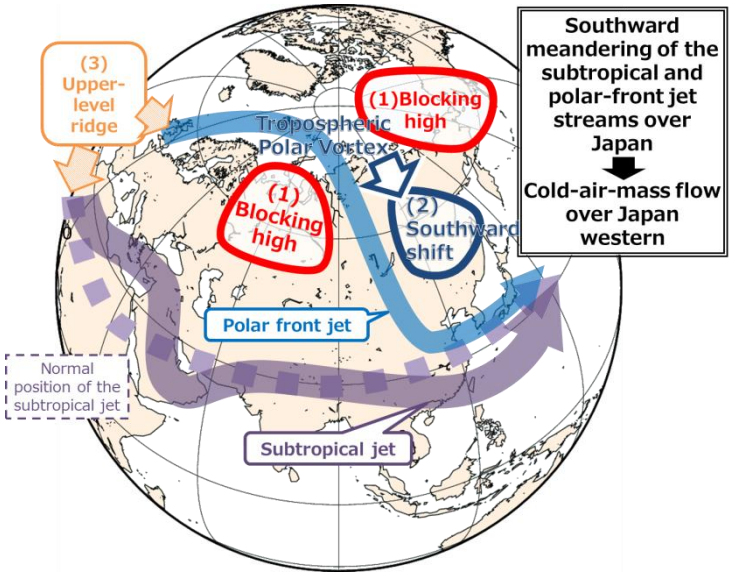

Figure 27 Primary factors behind the severe cold wave hitting Japan in early February 2018

When a severe cold wave hit western and other parts of Japan in early February 2018, the subtropical and polar front jet streams were exhibiting clear meandering over Eurasia. The numbered events in Figure 5 are described in further detail below.

(1) Blocking highs developed over the area from the Bering Sea to its north and over western Siberia.

(2) These highs caused a split in the tropospheric polar vortex, and one of the pieces was pushed toward eastern Siberia in association with the southward meandering of the polar front jet stream around Japan.

(3) The meandering of the subtropical and polar front jet streams was probably caused by Rossby wave packet propagation that can be traced back to the upper-level ridge over the North Atlantic.

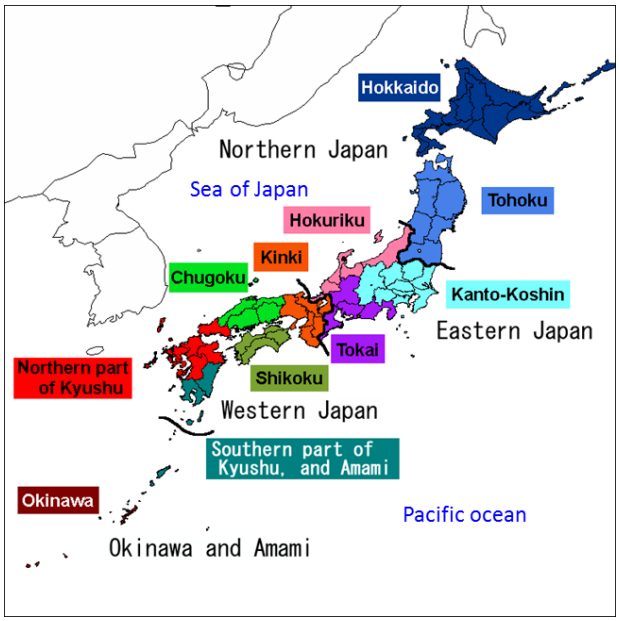

Figure 28 Climatological regions of Japan
The country has four divisions (northern, eastern, western Japan and Okinawa/Amami) and eleven subdivisions (Hokkaido, Tohoku, Kanto-koshin, Hokuriku, Tokai, Kinki, Chugoku, Shikoku, northern Kyushu, southern Kyushu and Okinawa).

World climate monitoring webpage revamp

TCC provides a range of climate-related products and tools via its website to support Asia-Pacific regional and national climate services in its role as a WMO Regional Climate Center (RCC) in Regional Association II (Asia).

In May 2018, the Center revamped the climate monitoring website to improve user accessibility and operability. The new extreme climate report content is visually simpler than before and provides direct links to temperature anomaly maps, extreme climate event distribution maps and other relevant resources. These maps were previously provided on individual report pages, but are now integrated into the site's World Climate Chart page for ease of viewing. They can also be accessed via the links on the right of extreme climate report pages.

The URL for weekly report, for example, is as follow;
http://ds.data.jma.go.jp/tcc/tcc/products/climate/weekly/index.html

TCC maintains its commitment to supporting operational climate monitoring activities at National Meteorological and Hydrological Services (NMHSs) via its website.

(Hirotaka Sato, Climate Prediction Division)

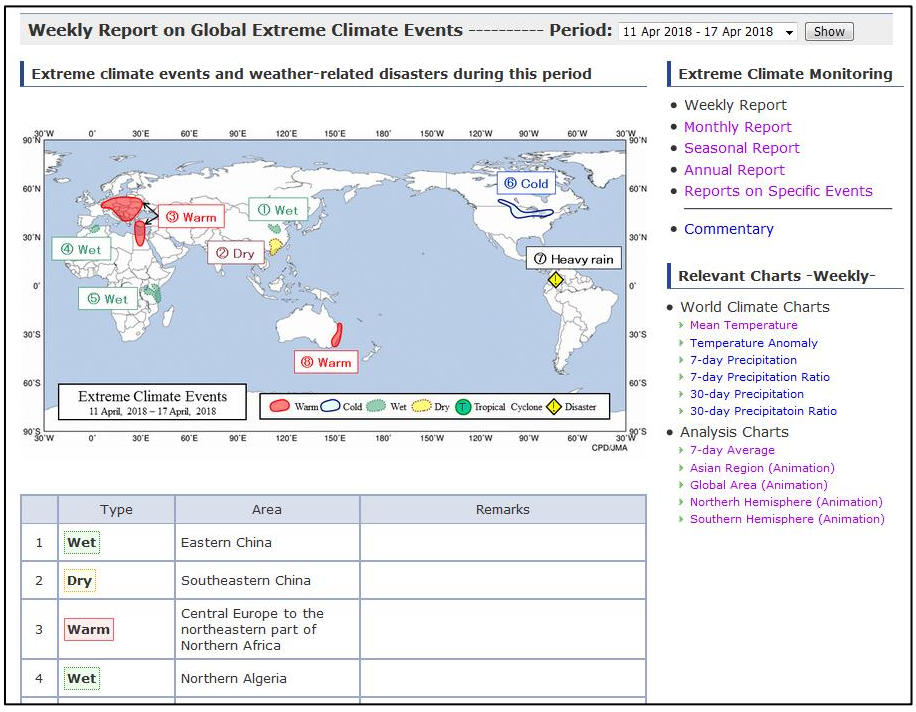

	Type	Area	Remarks
1	Wet	Eastern China	
2	Dry	Southeastern China	
3	Warm	Central Europe to the northeastern part of Northern Africa	
4	Wet	Northern Algeria	

A revamped webpage for weekly report on global extreme climate events

TCC contributions to Regional Climate Outlook Forums in Asia

WMO Regional Climate Outlook Forums (RCOFs) bring together national, regional and international climate experts on an operational basis to produce regional climate outlooks based on input from participating NMHSs, regional institutions, Regional Climate Centers and global producers of climate predictions. By providing a platform for countries with similar climatological characteristics to discuss related matters, these forums ensure consistency in terms of access to and interpretation of climate information. In spring 2018, TCC experts participated in two RCOFs in Asia.

1. FOCRA II

The first RCOF was held at the 14th session of the Forum on Regional Climate Monitoring, Assessment and Prediction for Regional Association II (FOCRA II) in Nanning, China, from 24 to 26 April. At the event, experts from 17 countries/territories made presentations in seven sessions featuring talks by invited lecturers and other oral presentations. TCC attendees gave two presentations outlining the characteristics of the last winter monsoon and the outlook for this summer based on JMA's seasonal Ensemble Prediction System (EPS). The presentations contributed to discussions on a consensus outlook for the coming summer.

2. SASCOF

The second RCOF was the 12th session of the South Asian Climate Outlook Forum (SASCOF-12) held in Pune, India, from 19 to 20 April. This forum is held twice a year to provide a consensus outlook for South Asian monsoon season. More than 30 experts from South Asian countries (Bangladesh, Bhutan, India, the Maldives, Myanmar, Nepal and Sri Lanka) and global centers attended the event, engaging in discussions on current/future climate conditions and developing a consensus outlook for the upcoming summer monsoon season (Jun. to Sep. 2018). The SASCOF consensus outlook is critically important for South Asian countries to prevent disasters caused by extreme climate events such as heavy rainfall and droughts.

As a contribution to such activities, one TCC expert participated in SASCOF-12 to provide predictions on oceanic and atmospheric conditions, including probabilistic forecasting of monsoon rainfall in South Asia based on JMA's seasonal EPS. The prediction was overall consistent with those based on other models and supported a decision on the consensus outlook.

(FOCRA II: Hiroshi Ohno and Mizuki Hanafusa, SASCOF-12: Atsushi Minami, Tokyo Climate Center)

Mizuki Hanafusa presents characteristics of the last winter monsoon (left) and Hiroshi Ohno presents seasonal forecast for this summer (right) at FOCRA II.

You can also find the latest newsletter from Japan International Cooperation Agency (JICA).

JICA's World (April 2018)
https://www.jica.go.jp/english/publications/j-world/c8h0vm0000chel5v-att/1804.pdf
JICA's World is the quarterly magazine published by JICA. It introduces various cooperation projects and partners along with the featured theme. The latest issue features "Change the Oceans, Change the World".

Any comments or inquiry on this newsletter and/or the TCC website would be much appreciated. Please e-mail to tcc@met.kishou.go.jp.

(Editors: Yasushi Takatsuki, Yasushi Mochizuki and Atsushi Minami)

Tokyo Climate Center (TCC), Japan Meteorological Agency
Address: 1-3-4 Otemachi, Chiyoda-ku, Tokyo 100-8122, Japan
TCC Website: http://ds.data.jma.go.jp/tcc/tcc/index.html